

Combined CDF and D0 upper limits on $gg \rightarrow H \rightarrow W^+W^-$ and constraints on the Higgs boson mass in fourth-generation fermion models with up to 8.2 fb^{-1} of data

The TEVNPH Working Group*

*for the CDF and D0 Collaborations**October 15, 2018*

We combine results from searches by the CDF and D0 Collaborations for a standard model Higgs boson (H) in the processes $gg \rightarrow H \rightarrow W^+W^-$ and $gg \rightarrow H \rightarrow ZZ$ in $p\bar{p}$ collisions at the Fermilab Tevatron Collider at $\sqrt{s} = 1.96 \text{ TeV}$. With 8.2 fb^{-1} of integrated luminosity analyzed at CDF and 8.1 fb^{-1} at D0, the 95% C.L. upper limit on $\sigma(gg \rightarrow H) \times \mathcal{B}(H \rightarrow W^+W^-)$ is 1.01 pb at $m_H = 120 \text{ GeV}$, 0.40 pb at $m_H = 165 \text{ GeV}$, and 0.47 pb at $m_H = 200 \text{ GeV}$. Assuming the presence of a fourth sequential generation of fermions with large masses, we exclude at the 95% Confidence Level a standard-model-like Higgs boson with a mass between 124 and 286 GeV.

Preliminary Results

* The Tevatron New-Phenomena and Higgs Working Group can be contacted at TEVNPHWG@fnal.gov. More information can be found at <http://tevnpwhg.fnal.gov/>.

I. INTRODUCTION

Exploring the mechanism for the breaking of the $SU(2) \times U(1)$ electroweak gauge symmetry is a priority in high energy physics. Not only are this symmetry and its breaking [1] necessary components for the consistency of the successful standard model (SM) [2], but measurable properties of the breaking mechanism are also very sensitive to possible phenomena that have not yet been observed at collider experiments. Measuring these properties, or setting limits on them, can constrain broad classes of extensions to the SM.

A natural extension to the SM that can be tested with Higgs boson search results at the Fermilab Tevatron Collider is the addition of a fourth generation of fermions with masses much larger than those of the three known generations [3]. While fits to precision electroweak data favor a low-mass Higgs boson in the SM, the addition of a fourth generation of fermions to the SM modifies the fit parameters such that a much heavier Higgs boson is allowed [4, 5]. Currently available data are consistent with a Higgs boson of mass 900 GeV with suitably chosen fourth generation fermion masses [6]. Precision measurements of the Z boson decay width [7] exclude models in which the fourth neutrino mass eigenstate has a mass less than 45 GeV. If the neutrino masses are very large, however, a fourth generation of fermions is not excluded.

One consequence of the extra fermions is that the ggH coupling is enhanced by a factor of roughly three relative to the SM coupling [5, 8, 9]. The reason for this is that the lowest-order ggH coupling arises from a quark loop. The top quark contribution is the largest due to its large coupling with the Higgs boson. In the limit $m_{q4} \gg m_H$ where m_{q4} is the fourth-generation quark mass, the Higgs boson coupling cancels the mass dependence for each of the three propagators in the loop, and the contribution to the ggH coupling becomes asymptotically independent of the masses of the two fourth-generation quarks. Each additional fourth-generation quark then contributes as much as the top quark, and the ggH coupling is thus enhanced by a factor K_e of approximately three.

The production cross section will be enhanced by a factor of K_e^2 . For m_H near the low end of our search range, $m_H \approx 110$ GeV, the $gg \rightarrow H$ production cross section is enhanced by roughly a factor of nine relative to the SM prediction. This factor drops to approximately 7.5 near the upper end of the search range, $m_H \approx 300$ GeV, assuming asymptotically large masses for the fourth-generation quarks. The reason for this drop is that the denominator of the enhancement factor, the SM cross section, has a larger contribution from the SM top quark as m_H nears $2m_t$. The partial decay width for $H \rightarrow gg$ is enhanced by the same factor as the production cross section. However, because the decay $H \rightarrow gg$ is loop-mediated, the $H \rightarrow W^+W^-$ decay continues to dominate for Higgs boson masses $m_H > 135$ GeV.

We consider two scenarios for the masses of the fourth-generation fermions. In the first scenario, the “low-mass” scenario, we set the mass of the fourth-generation neutrino $m_{\nu 4} = 80$ GeV, and the mass of the fourth-generation charged lepton $m_{\ell 4} = 100$ GeV, in order to evade experimental constraints [10] and to have the maximum impact on the Higgs boson decay branching ratios. In the second scenario, the “high-mass” scenario, we set $m_{\nu 4} = m_{\ell 4} = 1$ TeV, so that the fourth-generation leptons do not affect the decay branching ratios of the Higgs boson. In both scenarios, we choose the masses of the quarks to be those of the second scenario in Ref. [9], that is, we set the mass of the fourth-generation down-type quark to be $m_{d4} = 400$ GeV and the mass of the fourth-generation up-type quark to be $m_{u4} = m_{d4} + 50 \text{ GeV} + 10 \log(m_H/115 \text{ GeV}) \text{ GeV}$. The other mass spectrum of Ref. [9] chooses $m_{d4} = 300$ GeV, resulting in slightly larger predictions for $\sigma(gg \rightarrow H)$ and nearly identical decay branching ratios. We use the next-to-next-to-leading order (NNLO) production cross section calculation of Ref. [9], which builds on the NNLO SM calculations of Refs. [11–18].

The CDF and D0 Collaborations have searched for the SM Higgs boson in the decays $H \rightarrow W^+W^-$ and $H \rightarrow ZZ$ using all SM production processes: $gg \rightarrow H$, $qq \rightarrow WH$, $qq \rightarrow ZH$, and vector-boson fusion (VBF) [19–23]. The results of these searches for the SM Higgs boson cannot be used directly to constrain fourth-generation models, as the ggH coupling is enhanced but the WWH and ZZH couplings are not, and the signal acceptances and the backgrounds in the multiple analysis channels differ for the various production modes.

Previously, the CDF and D0 Collaborations have published searches for the process $gg \rightarrow H \rightarrow W^+W^-$, also neglecting the WH , ZH , and VBF signal contributions [24–26]. This paper is an update of Ref. [26], which provides a fourth-generation interpretation of the $gg \rightarrow H \rightarrow W^+W^-$ searches, and a model-independent limit on $\sigma(gg \rightarrow H \rightarrow W^+W^-)$. Here we update the searches detailed in Ref. [26] with those using 8.2 fb^{-1} from CDF [19] and 8.1 fb^{-1} from D0 [21] and include additional channels [20, 22, 23]. Interpretations of SM Higgs boson searches within

the context of a fourth generation of fermions have been performed by ATLAS [27] and CMS [28], which exclude $140 < m_H < 185$ GeV and $144 < m_H < 207$ GeV, respectively.

We present new limits on $\sigma(gg \rightarrow H) \times \mathcal{B}(H \rightarrow W^+W^-)$ in which the $gg \rightarrow H$ production mechanism is considered as the unique signal source. These limits are compared to models for Higgs boson production in which the ggH coupling is enhanced by the presence of a single additional generation of fermions. In this comparison, the decay branching ratios of the Higgs boson are also modified to reflect changes due to the fourth generation relative to the SM prediction. While the decays of the heavy quarks and leptons may include W bosons in the final state, we do not include these as additional sources of signal. The branching ratios for $H \rightarrow W^+W^-$ are calculated using HDECAY [29] modified to include fourth-generation fermions [5]. The modified Higgs branching ratio to W^+W^- is multiplied by the cross section [9] to predict the fourth-generation enhanced $gg \rightarrow H \rightarrow W^+W^-$ production rate. We include as an approximation to the uncertainties on the decay branching ratios the relative uncertainties predicted for the SM branching ratios due to uncertainties in m_b , m_c , and α_s presented in Ref. [30].

The branching ratio for the decay $H \rightarrow ZZ$ is also considerable at large masses, having a peak at around $m_H = 135$ GeV and rising above $m_H = 180$ GeV. In order to include a search for $gg \rightarrow H \rightarrow ZZ$, we introduce the assumption that $\mathcal{B}(H \rightarrow W^+W^-)/\mathcal{B}(H \rightarrow ZZ)$ remains as predicted by the SM, even though the production cross section is enhanced. This assumption holds true in fourth-generation models as predicted by the fourth-generation version of HDECAY mentioned above. In setting limits on $\sigma(gg \rightarrow H) \times \mathcal{B}(H \rightarrow W^+W^-)$, we include the process $gg \rightarrow H \rightarrow ZZ$ assuming that its signal yield scales in the same way as the W^+W^- channel.

The event selections are similar for the corresponding CDF and D0 analyses. Both collaborations select events with large \cancel{E}_T and two oppositely charged, isolated leptons, targeting the $H \rightarrow W^+W^-$ signal in which both W bosons decay leptonically. D0 selects events containing electrons and/or muons, dividing the data sample into three final states: e^+e^- , $e^\pm\mu^\mp$, and $\mu^+\mu^-$. Each final state is further subdivided according to the number of jets in the event: 0, 1, or 2 or more (“2+”) jets. However, in the fourth-generation interpretation and the model-independent $gg \rightarrow H$ limits, due to the low S/B in the 2-jet multiplicity bin, only the 0 and 1-jet multiplicity bins were taken into account. Decays involving tau leptons are included in two orthogonal ways. A dedicated analysis ($\mu\tau_{had}$) using 7.3 fb^{-1} of data studying the final state involving a muon and a hadronic tau decay, is included [22]. Final states involving other tau decays and mis-identified hadronic tau decays are included in the e^+e^- , $e^\pm\mu^\mp$, and $\mu^+\mu^-$ final state analyses. The CDF analysis separates opposite-sign candidate events into five non-overlapping channels. Events are classified by their jet multiplicity (0, 1, or ≥ 2), and the 0 and 1 jet channels are further divided according to whether both leptons are in the central part of the detector or if either lepton is in the forward part of the detector. The presence of neutrinos in the final state prevents event-by-event reconstruction of the Higgs boson mass and thus other variables are used for separating the signal from the background. For example, the angle $\Delta\phi(\ell, \ell)$ in signal events is smaller on average than that in background events, the missing transverse momentum is larger, and the total transverse energy of the jets is lower. The CDF analyses use neural-network (NN) outputs as the final discriminants; the list of network inputs includes likelihood ratio discriminant variables constructed from matrix-element probabilities [24]. The D0 e^+e^- , $e^\pm\mu^\mp$, and $\mu^+\mu^-$ final state channels use random forest boosted decision tree (BDT) outputs as the final discriminants while the $\mu\tau_{had}$ channel uses neural networks. Both experiments use separate NNs and BDTs for the different jet multiplicities to distinguish the $gg \rightarrow H$ signal from the backgrounds for each of the test masses, which are separated by increments of 5 or 10 GeV.

CDF introduces a search for $gg \rightarrow H \rightarrow ZZ \rightarrow \ell^+\ell^-\ell'^+\ell'^-$ using 8.2 fb^{-1} of data [20]. The discriminant variable is the reconstructed mass of the four leptons $m_{\ell\ell\ell\ell}$. The version of this search used for the Standard Model interpretation also includes the expected yield for WH , ZH , and VBF production, but these production modes are assumed not to contribute when interpreting the results in this paper.

D0 also includes for the first time channels in which one of the W bosons in the $H \rightarrow W^+W^-$ process decays leptonically and the other decays hadronically [23]. Electron and muon final states are studied separately, each with 5.3 fb^{-1} of data. Random forests are used for the final discriminants.

Both CDF and D0 conduct all searches included in this paper in the range $110 < m_H < 300$ GeV. The details of the signal and background estimations and the systematic uncertainties are provided in Refs. [19–23]. We set limits on $\sigma(gg \rightarrow H) \times \mathcal{B}(H \rightarrow W^+W^-)$ as a function of m_H . We use the same two statistical methods employed in Ref. [31], namely the modified frequentist (CL_s) and Bayesian techniques, in order to study the consistency of the results. Each method is applied at each test mass to calculate an observed upper limit on $\sigma(gg \rightarrow H) \times \mathcal{B}(H \rightarrow W^+W^-)$. Pseudo-experiments drawn from systematically varied background-only predictions are used to compute the limits we

expect to obtain in the absence of a signal.

Correlated systematic uncertainties are treated in the same way as they are in Ref. [31]. The sources of correlated uncertainty between CDF and D0 are the total inelastic $p\bar{p}$ cross section used in the luminosity measurement, the SM diboson background production cross sections (WW , WZ , and ZZ), and the $t\bar{t}$ and single top quark production cross sections. Instrumental effects such as trigger efficiencies, lepton identification efficiencies and misidentification rates, and the jet energy scales used by CDF and D0 remain uncorrelated. To minimize the degrading effects of systematics on the search sensitivity, the signal and background contributions are fit to the data observations by maximizing a likelihood function over the systematic uncertainties for both the background-only and signal+background hypotheses [32]. When setting limits on $\sigma(gg \rightarrow H) \times \mathcal{B}(H \rightarrow W^+W^-)$, we do not include the theoretical uncertainty on the prediction of $\sigma(gg \rightarrow H) \times \mathcal{B}(H \rightarrow W^+W^-)$ in the fourth-generation models since these limits are independent of the predictions. When setting limits on m_H in the context of fourth-generation models, however, we include the uncertainties on the theoretical predictions as described below.

Since both the CDF and the D0 analyses categorize events into separate channels based on the number of reconstructed jets, we include the systematic uncertainties on each jet category according to the procedure recommended by Ref. [33]. This procedure treats the factorization and renormalization scale uncertainties as independent in the inclusive $gg \rightarrow H$, $gg \rightarrow H + 1$ or more jets, and $gg \rightarrow H + 2$ or more jets calculations. We propagate these uncertainties through to the calculations of the exclusive $H + 0$ jets, $H + 1$ jet, and $H + 2$ or more jets calculations required to predict the yields in the fourth-generation models. When setting a limit on $\sigma(gg \rightarrow H \rightarrow W^+W^-)$, we do not include a theoretical uncertainty on the prediction of the quantity that we are constraining experimentally. Nonetheless, we do require theoretical input for the differential distributions of the number of jets in $gg \rightarrow H$ production. We therefore use only the factorization and renormalization scale uncertainties on the $H + 1$ or more jets and $H + 2$ or more jets inclusive calculations when setting a limit on the inclusive process. We follow the PDF4LHC prescription [34] for evaluating the parton distribution function (PDF) uncertainties on the signal predictions. QCD scale uncertainties that affect the PDF predictions are included as part of the total scale uncertainty, added linearly to the other components of the scale uncertainty. The remaining component of the PDF uncertainty is treated as uncorrelated with the QCD scale uncertainty.

The scale choice affects the p_T spectrum of the Higgs boson when produced in gluon-gluon fusion, and this effect changes the acceptance of the selection requirements and also the shapes of the distributions of the final discriminants. The effect of the acceptance change is included in the calculations of Ref. [35] and Ref. [36], as the experimental requirements are simulated in these calculations. The effects on the final discriminant shapes are obtained by reweighting the p_T spectrum of the Higgs boson production in our Monte Carlo simulation to higher-order calculations. The Monte Carlo signal simulation used by CDF and D0 is provided by the LO generator PYTHIA [37] which includes a parton shower and fragmentation and hadronization models. We reweight the Higgs boson p_T spectra in our PYTHIA Monte Carlo samples to that predicted by HQT [38] when making predictions of differential distributions of $gg \rightarrow H$ signal events. To evaluate the impact of the scale uncertainty on our differential spectra, we use the RESBOS [39] generator, and apply the scale-dependent differences in the Higgs boson p_T spectrum to the HQT prediction, and propagate these to our final discriminants as a systematic uncertainty on the shape, which is included in the calculation of the limits.

The combined limits on $\sigma(gg \rightarrow H) \times \mathcal{B}(H \rightarrow W^+W^-)$ are listed in Table II for both the CL_s and the Bayesian methods, and are shown in Fig. 1 along with the fourth-generation theory predictions for the high-mass and low-mass scenarios. The uncertainty bands shown on the low-mass theoretical prediction are the quadrature sum of the MSTW 2008 [40] 90% C.L. PDF uncertainties and the factorization and renormalization scale uncertainties from Table 1 of Ref. [9]. The limits calculated with the two statistical methods agree within 10% for all Higgs boson mass hypotheses. An excess is seen in the neighborhood of $m_H = 140$ GeV. This excess is localized to the D0 $H \rightarrow W^+W^- \rightarrow e^+\nu_e\mu^-\bar{\nu}_\mu$ search (including charge conjugate final states) [21]. The excess is not as pronounced in the SM-optimized search from D0 [21]. Combination with CDF, which sees no significant excess at $m_H = 140$ GeV [19] results in a total local significance somewhat in excess of two standard deviations. The trials factor, or look-elsewhere effect, further dilutes the significance, in this case by a large factor due to the large range of m_H explored. We do not claim that this excess is statistically significant.

In order to set limits on m_H in these two scenarios, we perform a second combination, including the uncertainties on the theoretical predictions of $\sigma(gg \rightarrow H) \times \mathcal{B}(H \rightarrow W^+W^-)$ due to scale and PDF uncertainties at each value of m_H tested. The resulting limits are computed relative to the model prediction, and are shown in Fig. 2 for the low-mass scenario, which gives the smaller excluded range of m_H . In this scenario, we exclude at the 95% C.L. a SM-like

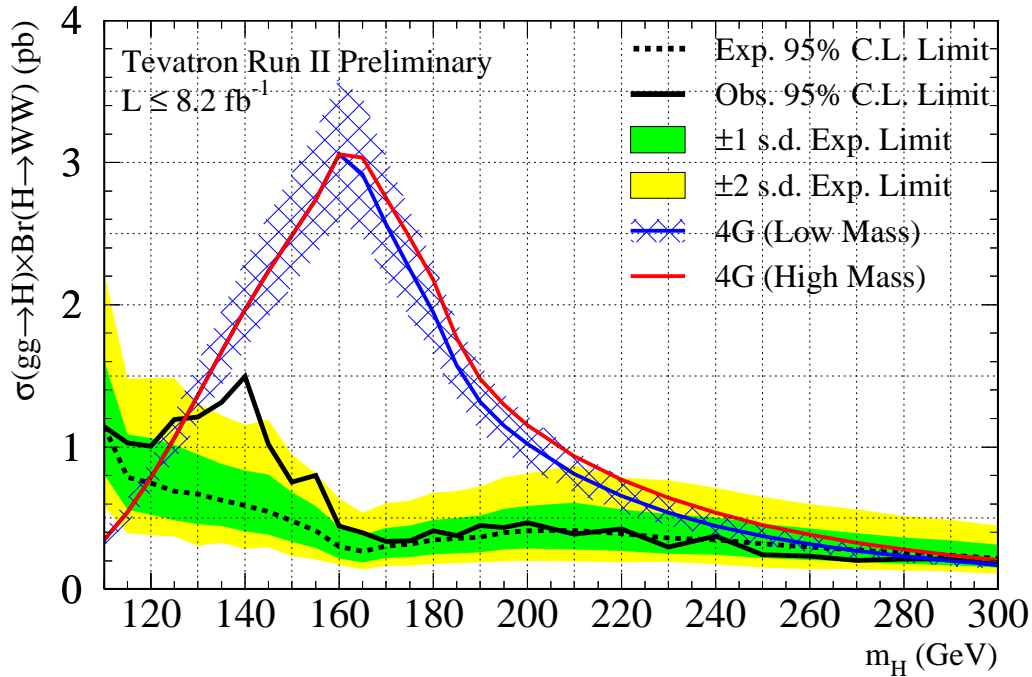


FIG. 1: The Tevatron combined observed (solid black lines) and median expected (dashed black lines) 95% C.L. upper limits on $\sigma(gg \rightarrow H) \times \mathcal{B}(H \rightarrow W^+W^-)$. The shaded bands indicate the ± 1 standard deviation (s.d.) and ± 2 s.d. intervals on the distribution of the limits that are expected if a Higgs boson signal is not present. Also shown the prediction for a fourth-generation model in the low-mass and high-mass scenarios, 4G (Low mass) and 4G (High mass) respectively. The hatched areas indicate the theoretical uncertainty from PDF and scale uncertainties. The lighter curves show the high-mass theoretical prediction.

Higgs boson with a mass in the range 124 – 286 GeV. Using the median limits on $\sigma(gg \rightarrow H) \times \mathcal{B}(H \rightarrow W^+W^-)$, expected in the absence of a signal to quantify the sensitivity, we expect to exclude the mass range 120 – 267 GeV. In the high-mass scenario, which predicts a larger $\mathcal{B}(H \rightarrow W^+W^-)$ at high m_H than that predicted in the low-mass scenario, we exclude at the 95% C.L. the mass range 124 – 300 GeV and expect to exclude the mass range 120 – 290 GeV. The upper edge of the observed exclusion range in the high-mass scenario is determined by the fact that we did not perform the search for Higgs bosons with mass exceeding 300 GeV.

In summary, we present a combination of CDF and D0 searches for the $gg \rightarrow H \rightarrow W^+W^-$ and $gg \rightarrow H \rightarrow ZZ$ processes and set an upper limit on $\sigma(gg \rightarrow H) \times \mathcal{B}(H \rightarrow W^+W^-)$ as a function of m_H , assuming the standard model ratio of $\mathcal{B}(H \rightarrow W^+W^-)/\mathcal{B}(H \rightarrow ZZ)$. We compare these limits with the prediction of the minimal SM with a sequential fourth generation of heavy fermions added on, and exclude at the 95% C.L. the Higgs boson mass range $124 < m_H < 286$ GeV, with an expected exclusion of 120 – 267 GeV.

Acknowledgements

We thank the Fermilab staff and the technical staffs of the participating institutions for their vital contributions. This work was supported by DOE and NSF (USA), CONICET and UBACyT (Argentina), CNPq, FAPERJ, FAPESP and FUNDUNESP (Brazil), CRC Program, CFI, NSERC and WestGrid Project (Canada), CAS and CNSF (China), Colciencias (Colombia), MSMT and GACR (Czech Republic), Academy of Finland (Finland), CEA and CNRS/IN2P3 (France), BMBF and DFG (Germany), Ministry of Education, Culture, Sports, Science and Technology (Japan), World Class University Program, National Research Foundation (Korea), KRF and KOSEF (Korea), DAE and DST

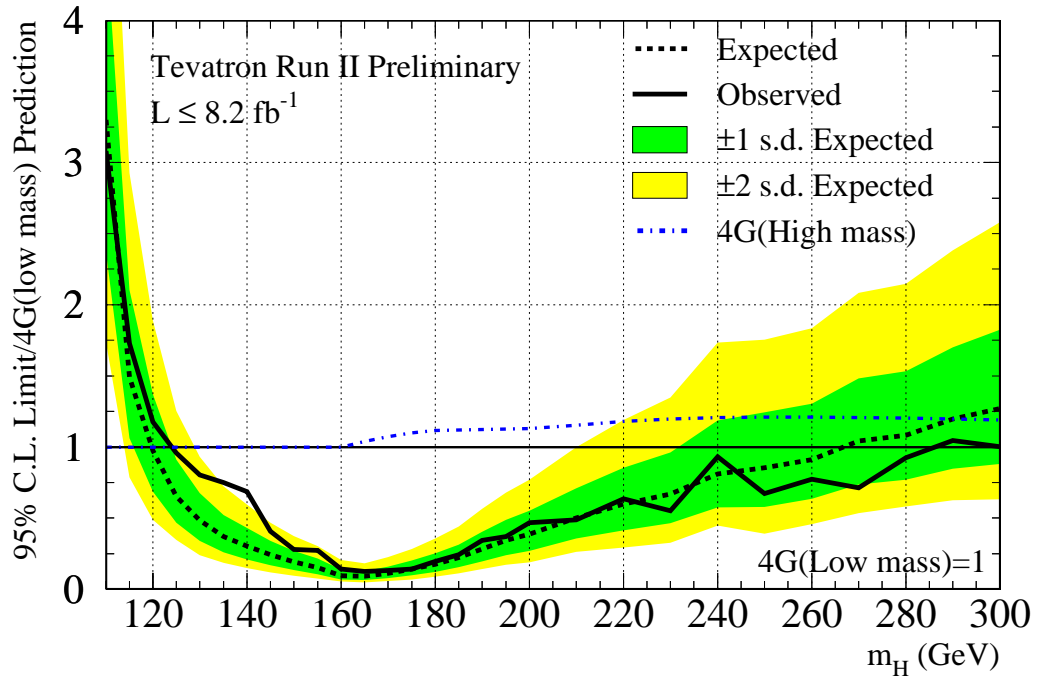


FIG. 2: The Tevatron combined observed (solid black lines) and median expected (dashed black lines) 95% C.L. upper limits on the ratio of the Higgs boson production cross section to that predicted by the 4G (Low mass) model; the uncertainties in the signal prediction are included in the limit. Also shown is the prediction of the signal rate in the high-mass scenario, divided by that of the low-mass scenario.

(India), SFI (Ireland), INFN (Italy), CONACyT (Mexico), NSC(Republic of China), FASI, Rosatom and RFBR (Russia), Slovak R&D Agency (Slovakia), Ministerio de Ciencia e Innovación, and Programa Consolider-Ingenio 2010 (Spain), The Swedish Research Council (Sweden), Swiss National Science Foundation (Switzerland), FOM (The Netherlands), STFC and the Royal Society (UK), and the A.P. Sloan Foundation (USA).

-
- [1] P.W. Higgs, Phys. Lett. **12** (1964) 132; *idem*, Phys. Rev. Lett. **13** (1964) 508; *idem*, Phys. Rev. **145** (1966) 1156; F. Englert and R. Brout, Phys. Rev. Lett. **13** (1964) 321; G. S. Guralnik, C. R. Hagen and T. W. B. Kibble, Phys. Rev. Lett. **13** (1964) 585.
- [2] S. L. Glashow, Nucl. Phys. **22**, 579 (1961); S. Weinberg, Phys. Rev. Lett. **19** (1967) 1264; A. Salam, *Elementary Particle Theory*, ed. N. Svartholm (Almqvist and Wiksells, Stockholm, 1968), 367.
- [3] B. Holdom, *et al.*, PMC Phys. A **3**, 4 (2009).
- [4] H. J. He, N. Polonsky and S. f. Su, Phys. Rev. D **64**, 053004 (2001).
- [5] G. D. Kribs, T. Plehn, M. Spannowsky, and T. M. P. Tait, Phys. Rev. D **76**, 075016 (2007).
- [6] M. Baak *et al.*, arXiv:1107.0975 [hep-ph] (2011).
- [7] The ALEPH, DELPHI, L3, OPAL, SLD Collaborations, the LEP Electroweak Working Group, and the SLD Electroweak and Heavy Flavor Groups, Phys. Rept. **427**, 257 (2006).
- [8] E. Arik, O. Cakir, S. A. Cetin, and S. Sultansoy, Acta Phys. Pol. B **37**, 2839 (2006).
- [9] C. Anastasiou, R. Boughezal, and E. Furlan, arXiv:1003.4677 [hep-ph] (2010).
- [10] P. Achard *et al.* [L3 Collaboration], Phys. Lett. B **517**, 75 (2001).

- [11] R. V. Harlander and W. B. Kilgore, Phys. Rev. Lett. **88**, 201801 (2002).
- [12] C. Anastasiou and K. Melnikov, Nucl. Phys. B **646**, 220 (2002).
- [13] V. Ravindran, J. Smith, and W. L. van Neerven, Nucl. Phys. B **665**, 325 (2003).
- [14] C. Anastasiou, R. Boughezal, and F. Petriello, J. High Energy Phys. **0904**, 003 (2009).
- [15] C. Anastasiou, S. Bucherer, and Z. Kunszt, J. High Energy Phys. **0910**, 068 (2009).
- [16] M. Spira, A. Djouadi, D. Graudenz, and P. M. Zerwas, Nucl. Phys. B **453**, 17 (1995).
- [17] S. Catani, D. de Florian, M. Grazzini, and P. Nason, J. High Energy Phys. **0307**, 028 (2003).
- [18] U. Aglietti, R. Bonciani, G. Degrossi, and A. Vicini, Phys. Lett. B **595**, 432 (2004).
- [19] CDF Collaboration, “Search for $H \rightarrow WW^*$ Production at CDF Using 8.2 fb⁻¹ of Data”, CDF Note 10599 (2011).
- [20] CDF Collaboration, “A Search for the Higgs Boson in the Four Lepton Final State”, CDF Note 10573 (2011).
- [21] D0 Collaboration, “Search for Higgs boson production in dilepton plus missing energy final states with 8.1 fb⁻¹ of $p\bar{p}$ collisions at $\sqrt{s} = 1.96$ TeV”, D0 Conference Note 6219.
- [22] D0 Collaboration, “Search for the Standard Model Higgs boson in $\mu + \tau_{had} \leq 1$ jet final state with 7.3 fb⁻¹ of data”, D0 Conference Note 6179.
- [23] D0 Collaboration, “A search for the standard model Higgs boson in the $H \rightarrow WW \rightarrow \ell\nu q\bar{q}'$ Decay Channel”, Phys. Rev. Lett. **106**, 171802 (2011).
- [24] T. Aaltonen *et al.* [CDF Collaboration], Phys. Rev. Lett. **104**, 061803 (2010).
- [25] V. M. Abazov *et al.* [D0 Collaboration], Phys. Rev. Lett. **104**, 061804 (2010).
- [26] T. Aaltonen *et al.* [CDF and D0 Collaborations], Phys. Rev. D **82**, 011102 (2010).
- [27] ATLAS Collaboration, G. Aad *et al.*, arXiv:1106.2748, CERN-PH-EP-2011-076 (2011).
- [28] CMS Collaboration, S. Chatrchyan *et al.*, Phys. Lett. B **699**, 25 (2011).
- [29] A. Djouadi, J. Kalinowski, and M. Spira, Comput. Phys. Commun. **108**, 56 (1998).
- [30] J. Baglio, A. Djouadi, JHEP **1103**, 055 (2011). [arXiv:1012.0530 [hep-ph]].
- [31] T. Aaltonen *et al.* [CDF and D0 Collaborations], Phys. Rev. Lett. **104**, 061802 (2010).
- [32] C. Amsler *et al.* (Particle Data Group), Phys. Lett. B **667**, 1 (2008); W. Fisher, FERMILAB-TM-2386-E.
- [33] I. W. Stewart, F. J. Tackmann, [arXiv:1107.2117 [hep-ph]].
- [34] <http://www.hep.ucl.ac.uk/pdf4lh/>;
S. Alekhin *et al.*, (PDF4LHC Working Group), [arXiv:1101.0536v1 [hep-ph]];
M. Botje *et al.*, (PDF4LHC Working Group), [arXiv:1101.0538v1 [hep-ph]].
- [35] C. Anastasiou, G. Dissertori, M. Grazzini, F. Stöckli, and B. R. Webber, J. High Energy Phys. **0908**, 099 (2009).
- [36] J. M. Campbell, R. K. Ellis, C. Williams, Phys. Rev. **D81**, 074023 (2010). [arXiv:1001.4495 [hep-ph]].
- [37] T. Sjöstrand, L. Lonnblad and S. Mrenna, “PYTHIA 6.2: Physics and manual,” arXiv:hep-ph/0108264.
- [38] G. Bozzi, S. Catani, D. de Florian, and M. Grazzini, Phys. Lett. B **564**, 65 (2003); // G. Bozzi, S. Catani, D. de Florian, and M. Grazzini, Nucl. Phys. B **737**, 73 (2006).
- [39] C. Balazs, J. Huston, I. Puljak, Phys. Rev. D **63** 014021 (2001).
C. Balazs and C.-P. Yuan, Phys. Lett. B **478** 192-198 (2000).
Qing-Hong Cao and Chuan-Ren Chen, Phys. Rev. D **76** 073006 (2007).
- [40] A. D. Martin, W. J. Stirling, R. S. Thorne, and G. Watt, Eur. Phys. J. C **64**, 653 (2009).

TABLE I: The fourth-generation enhanced $\sigma(gg \rightarrow H)$ listed in fb for the low-mass scenario described in the text with $m_{d4} = 300$ GeV and $m_{d4} = 400$ GeV along with the $\mathcal{B}(H \rightarrow W^+W^-)$ for Higgs masses between 110 - 300 GeV. The uncertainty on the predicted cross section from variations in the PDF and factorization and renormalization scale are also listed in percentage where these have been determined from the MSTW 2008 90% C.L. uncertainty and by modification of the scale by factors of 1/2 and 2, respectively. The inclusive uncertainties are listed here, but the differential uncertainties in the jet categories are used in the calculation of the limits.

m_H (GeV)	$\sigma(gg \rightarrow H)$ $m_{d4} = 300$ GeV	$\sigma(gg \rightarrow H)$ $m_{d4} = 400$ GeV	uncert. PDF up(%)	uncert. PDF down(%)	uncert. μ up(%)	uncert. μ down(%)	$BR(H \rightarrow W^+W^-)$ $m_{d4} = 300$ GeV	$BR(H \rightarrow W^+W^-)$ $m_{d4} = 400$ GeV
110	12384	12308	12	-11	12	-8	0.028	0.028
115	10798	10725	12	-11	12	-8	0.050	0.051
120	9449.9	9384.3	12	-11	12	-8	0.083	0.083
125	8298.8	8240.0	12	-12	12	-8	0.13	0.13
130	7314.0	7258.7	12	-12	12	-8	0.19	0.19
135	6465.1	6414.2	12	-12	12	-8	0.26	0.26
140	5731.4	5684.1	13	-12	12	-8	0.35	0.35
145	5094.6	5050.4	13	-12	12	-8	0.44	0.44
150	4540.5	4498.5	13	-12	12	-8	0.55	0.55
155	4055.6	4017.6	13	-12	12	-8	0.68	0.68
160	3630.2	3595.1	13	-13	12	-8	0.85	0.85
165	3253.7	3220.7	14	-13	12	-8	0.91	0.91
170	2924.1	2893.2	14	-13	12	-8	0.89	0.88
175	2633.9	2604.4	14	-13	12	-8	0.86	0.86
180	2376.7	2348.9	14	-13	12	-8	0.83	0.83
185	2147.2	2121.5	15	-13	12	-8	0.74	0.74
190	1943.9	1919.7	15	-14	12	-8	0.69	0.69
195	1763.2	1740.2	15	-14	12	-8	0.66	0.66
200	1601.8	1580.0	15	-14	12	-8	0.65	0.65
210	1328.1	1308.4	16	-14	12	-8	0.62	0.62
220	1107.7	1089.6	16	-15	12	-8	0.60	0.60
230	928.61	912.21	17	-15	12	-8	0.59	0.59
240	782.52	767.44	17	-15	12	-8	0.58	0.58
250	662.60	648.81	18	-16	12	-8	0.58	0.58
260	563.53	550.90	19	-16	12	-8	0.57	0.58
270	481.49	469.93	19	-16	12	-8	0.57	0.57
280	413.24	402.68	20	-17	12	-8	0.58	0.58
290	356.39	346.53	21	-17	12	-8	0.58	0.58
300	308.70	299.71	21	-17	12	-8	0.58	0.58

TABLE II: The observed and median expected 95% C.L. upper limits on $\sigma(gg \rightarrow H) \times \mathcal{B}(H \rightarrow W^+W^-)$ for m_H between 110 GeV and 300 GeV, obtained with the Bayesian and CL_s methods. Also listed are the $\sigma(gg \rightarrow H) \times \mathcal{B}(H \rightarrow W^+W^-)$ predictions of the low-mass and the high-mass fourth-generation scenarios discussed in the text for a fourth-generation down-type quark mass of 400 GeV. All limits and predictions are presented in pb.

m_H [GeV]	Obs.	Bayes		Ratio Low Mass (Exp./4Gen)	CL _s		4 th Gen	4 th Gen
		Ratio Low Mass (Obs./4Gen)	Exp.		Obs.	Exp.	Low Mass	High Mass
110	1.14	3.08	1.14	3.30			0.34	0.35
115	1.03	1.73	0.79	1.49	1.04	0.80	0.54	0.54
120	1.01	1.18	0.75	0.98	1.00	0.75	0.78	0.78
125	1.19	0.96	0.69	0.65	1.15	0.70	1.06	1.06
130	1.21	0.80	0.67	0.48	1.17	0.67	1.36	1.36
135	1.31	0.75	0.63	0.37	1.28	0.63	1.67	1.67
140	1.50	0.68	0.59	0.30	1.41	0.59	1.96	1.96
145	1.02	0.41	0.55	0.24	0.94	0.54	2.25	2.24
150	0.75	0.28	0.48	0.19	0.73	0.49	2.49	2.49
155	0.8	0.27	0.41	0.15	0.76	0.42	2.74	2.74
160	0.44	0.14	0.30	0.095	0.42	0.30	3.06	3.06
165	0.4	0.12	0.27	0.090	0.36	0.27	2.92	3.03
170	0.34	0.13	0.30	0.11	0.34	0.30	2.57	2.76
175	0.34	0.14	0.32	0.14	0.33	0.33	2.25	2.47
180	0.41	0.20	0.35	0.18	0.40	0.35	1.96	2.17
185	0.38	0.24	0.36	0.22	0.37	0.37	1.57	1.76
190	0.45	0.34	0.37	0.28	0.46	0.38	1.32	1.48
195	0.44	0.37	0.40	0.34	0.43	0.41	1.15	1.30
200	0.47	0.47	0.41	0.39	0.47	0.43	1.02	1.15
210	0.39	0.49	0.41	0.50	0.39	0.42	0.81	0.94
220	0.42	0.63	0.39	0.60	0.43	0.42	0.65	0.77
230	0.30	0.55	0.36	0.67	0.29	0.37	0.54	0.64
240	0.37	0.93	0.35	0.81	0.40	0.37	0.45	0.54
250	0.24	0.67	0.32	0.86	0.25	0.33	0.37	0.45
260	0.23	0.77	0.30	0.91	0.24	0.31	0.32	0.38
270	0.20	0.71	0.28	1.04	0.21	0.29	0.27	0.33
280	0.21	0.92	0.25	1.08	0.22	0.26	0.23	0.28
290	0.21	1.05	0.24	1.20	0.21	0.24	0.20	0.24
300	0.17	1.00	0.22	1.27	0.17	0.22	0.17	0.21